Water Oxidation by $[(tpy)(H_2O)_2Ru^{III}ORu^{III}(H_2O)_2(tpy)]^{4+}$

Estelle L. Lebeau, S. Ajao Adeyemi, and Thomas J. Meyer*

Department of Chemistry, CB#3290, Venable Hall, The University of North Carolina, Chapel Hill, North Carolina 27599-3290

Received July 24, 1997

The complex $[(tpy)(C_2O_4)Ru^{III}ORu^{III}(C_2O_4)(tpy)]\cdot 8H_2O$ (**1**·$8H_2O$) (tpy is 2,2′:6′,2″-terpyridine) has been prepared and characterized by X-ray crystallography and FTIR, resonance Raman, and ^{1}H NMR spectroscopies. From the results of the X-ray analysis, ∠RuORu is 148.5° with a torsional angle ($O_{22}-Ru_2-O_1-Ru_1-O_{12}$) of 22.7° and there is a short Ru−O bridge distance of 1.843 Å. **1** undergoes a chemically reversible one-electron, pH-independent oxidation at 0.73 V vs NHE (0.49 V vs SCE) from pH = 4−8 and a pH-dependent, two-electron, chemically irreversible reduction at −0.35 V below pH = 4.0. Addition of **1**·$8H_2O$ to strong acid generates $[(tpy)(H_2O)_2Ru^{III}ORu^{III}(H_2O)_2(tpy)]^{4+}$ (**2**), which has been characterized by UV−visible, resonance Raman, and ^{1}H NMR measurements. In pH-dependent cyclic voltammograms there is evidence for a series of redox couples interrelating oxidation states from $Ru^{II}ORu^{II}$ to $Ru^{V}ORu^{V}$. In contrast to the "blue dimer", *cis,cis*-$[(bpy)_2(H_2O)Ru^{III}ORu^{III}(OH_2)(bpy)_2]^{4+}$, oxidation state $Ru^{IV}ORu^{IV}$ ($Ru^{V}ORu^{III}$?) does appear as a stable oxidation state. Oxidation of $Ru^{IV}ORu^{IV}$ by Ce^{IV} in 0.1 M $HClO_4$ is followed by rapid O_2 production and appearance of an anated form of $Ru^{IV}ORu^{IV}$. O_2 formation is in competition with oxidative cleavage of $Ru^{V}ORu^{V}$ by Ce^{IV} to give $[Ru^{VI}(tpy)(O)_2(OH_2)]^{2+}$. Anation and oxidative cleavage prevent this complex from being a true catalyst for water oxidation.

Introduction

Oxidation of water to dioxygen is the terminal reaction of Photosystem II.[1−7] Although much has been learned about this system, little is known about how O_2 is evolved. There are a few well-defined molecules which effect this conversion,[5,7−18] one being the "blue dimer", *cis,cis*-$[(bpy)_2(H_2O)Ru^{III}ORu^{III}(OH_2)(bpy)_2]^{4+}$, and some of its derivatives. They are important because they have provided insights into possible mechanisms for water oxidation.[19−22] Activation occurs by oxidation with proton loss, which occurs sequentially, ultimately to give *cis,cis*-$[(bpy)_2(O)Ru^{V}ORu^{V}(O)(bpy)_2]^{4+}$.[23] Elucidation of the water oxidation mechanism has proven difficult because it involves five different oxidation states and cross reactions between them. Structures of *cis,cis*-$[(bpy)_2(H_2O)Ru^{III}ORu^{III}(OH_2)(bpy)_2]^{4+}$ and its once-oxidized form, $[(bpy)_2(OH)Ru^{IV}ORu^{III}(OH)(bpy)_2]^{4+}$, have been determined by X-ray crystallography.[12,14−16] The $Ru^{V}ORu^{V}$ form has been observed as a suspension, and resonance Raman measurements point to retention of the RuORu core and the presence of terminal Ru=O groups.[20]

This paper describes an extension of the water oxidation chemistry to a slightly modified structural motif based on $[(tpy)(H_2O)_2Ru^{III}ORu^{III}(H_2O)_2(tpy)]^{4+}$ (tpy is 2,2′,6′,2″-terpyridine) in which the μ-oxo core is retained but there are two additional water molecules at each ruthenium.

Experimental Section

Materials. $RuCl_3\cdot 3H_2O$ was purchased from Aldrich Chemical Co. 2,2′:6′,2″-terpyridine, $(NH_4)_2Ce(NO_3)_6$, and perchloric acid (70%) were purchased from G. F. Smith Chemicals. High-purity, deionized water was obtained by passing distilled water through a Nanopure (Barnstead) water purification system. High-purity NMR solvents were obtained from Cambridge Isotope Laboratories and used as received. HPLC grade water used for oxygen evolution experiments was obtained from Fisher. Trifluoromethanesulfonic (triflic) acid was obtained in 10-g ampules from Aldrich. All other common reagents were ACS grade and were used without additional purification.

Elemental Analysis. Microanalyses were conducted by Oneida Research Services, Inc., Whitesboro, NY.

(1) Brudvig, G. W.; Crabtree, R. H. *Proc. Natl. Acad. Sci. U.S.A.* **1986**, *83*, 4586.
(2) Brudvig, G. W.; Crabtree, R. H. *Prog. Inorg. Chem.* **1989**, *37*, 99.
(3) Christou, G. *Acc. Chem. Res.* **1989**, *22*, 324.
(4) Pecoraro, V. L. *Photochem. Photobiol.* **1988**, *48*, 249.
(5) Wieghardt, K. *Angew. Chem., Int. Ed. Engl.* **1989**, *28*, 1153.
(6) DeRose, V. J.; Mukerji, I.; Latimer, M. J.; Yachandra, V. K.; Sauer, K.; Klein, M. P. *J. Am. Chem. Soc.* **1994**, *116*, 5239.
(7) Pecoraro, V. L.; Baldwin, M. J.; Gelasco, A. *Chem. Rev.* **1994**, *94*, 4, 807−826.
(8) Debus, R. J. *Biochim. Biophys. Acta* **1992**, *1102*, 269−352.
(9) Wang, S.; Tsai, H.-L.; Libby, E.; Folting, K.; Streib, W. E.; Hendrickson, D. N.; Christou, G. *Inorg. Chem.* **1996**, *35*, 7578−7589.
(10) *Manganese Redox Enzymes*; Pecoraro, V. L., Ed.; Verlag Chemie: Weinheim, Germany, 1992.
(11) Prosperpio, D. M.; Hoffmann, R.; Dismukes, G. C. *J. Am. Chem. Soc.* **1992**, *114*, 4374−4382.
(12) Gilbert, J. A.; Eggleston, D. S.; Murphy, W. R., Jr.; Geselowitz, D. A.; Gersten, S. W.; Hodgson, D. J.; Meyer, T. J. *J. Am. Chem. Soc.* **1985**, *107*, 3855−3864.
(13) Lippard, S. J. *Angew. Chem., Int. Ed. Engl.* **1988**, *27*, 344−361.
(14) Gilbert, J. A.; Geselowitz, D.; Meyer, T. J. *J. Am. Chem. Soc.* **1986**, *108*, 1493−1501.
(15) Raven, S. J.; Meyer, T. J. *Inorg. Chem.* **1988**, *27*, 4478−4483.
(16) Schoonover, J. R.; Ni, J.; Roecker, L.; White, P. S.; Meyer, T. J. *Inorg. Chem.* **1996**, *35*, 5885−5892.
(17) Rüttinger, W.; Dismukes, G. C. *Chem. Rev.* **1997**, *97*, 1−24.
(18) Manchanda, R.; Brudvig, G.; Crabtree, R. H. *Coord. Chem. Rev.* **1995**, *144*, 1−38.
(19) Chronister, C. W.; Binstead, R. A.; Ni, J.; Meyer, T. J. *Inorg. Chem.* **1997**, *36*, 3814−3815.
(20) Lei, Y.; Hurst, J. K. *Inorg. Chim. Acta* **1994**, *226*, 179−185.
(21) Comte, P.; Nazeeruddin, M. K.; Rotzinger, F. P.; Frank, A. J.; Grätzel, M. *J. Mol. Catal.* **1989**, *52*, 63−84.
(22) Geselowitz, D.; Meyer, T. J. *Inorg. Chem.* **1990**, *29*, 3894−3896.
(23) Because of strong electronic coupling between the metal centers across the μ-oxo bridge, the shorthand notation adopted here for describing the oxidation states of the dimer is merely a convenience and may not accurately represent the detailed electronic structure. For example, if the odd electron in the $Ru^{III}ORu^{IV}$ dimer is delocalized, a more appropriate description is $Ru^{III.V}ORu^{III.V}$.

10.1021/ic970908z CCC: $15.00
Published on Web 11/19/1998

Preparations. $[Ru(tpy)(Cl)_3]$[24] and $[Ru(tpy)(C_2O_4)(H_2O)]\cdot 2H_2O$[25,26] were prepared by using literature methods.

$[(tpy)(C_2O_4)Ru^{III}ORu^{III}(C_2O_4)(tpy)]\cdot 8H_2O$ (1·8H$_2$O). A 1.0-g (2.28-mmol) quantity of freshly prepared $[Ru^{II}(tpy)(C_2O_4)(H_2O)]\cdot 2H_2O$ was suspended in 350 mL of nanopure water. The reaction mixture was heated at reflux with constant sparging by dioxygen for 5−8 h to form the blue μ-oxo complex. The progress of the reaction was monitored by UV−visible spectroscopy by observation of the growth of new bands for the dimer at 636 nm and for $[(tpy)(C_2O_4)Ru^{III}ORu^{IV}(tpy)(H_2O)$-$ORu^{III}(C_2O_4)(tpy)]^{2+}$ at 708 nm.[27] The reaction was terminated when there was no further evidence of the starting complex, $\lambda_{max} = 528$ and 580 nm. At this point the solution was filtered hot to remove any unreacted solid, the filtrate was reduced in volume to 50 mL on a steam bath, and the remaining solution was allowed to sit overnight in a refrigerator to achieve crystal formation. The dark blue microcrystals that appeared were filtered and washed several times with ice cold water until only the band at $\lambda_{max} = 636$ nm appeared in the filtrate washings. If $[(tpy)(C_2O_4)Ru^{III}ORu^{IV}(tpy)(H_2O)ORu^{III}(C_2O_4)(tpy)]^{2+}$ were present, it was removed by dissolving the blue solid in a minimum amount of water and purification by column chromatography by using Sephadex LH-20 and water as the eluent. The blue fraction ($\lambda_{max} = 636$ nm) was collected, and the solution was evaporated to 25 mL on a rotary evaporator and refrigerated overnight to obtain dark blue crystals. Yield: 63%. Anal. Calcd for $C_{34}H_{42}N_6O_{17}Ru_2$: C, 40.63; H, 4.18; N, 8.37. Found: C, 41.06; H, 3.79; N, 8.37. ^{1}H NMR spectrum in D_2O (diamagnetic): 8.29 (d, $J_{56} = 8.5$ Hz, 2 H, H_6, $H_{6''}$), 7.45 ppm (multiplet, 4 H, H_5, $H_{5''}$, $H_{3'}$, $H_{5'}$), 7.11 (ddd, $J_{45} = 6.25$ Hz $J_{34} = 5$ Hz, $J_{46} = 1.25$ Hz, 2 H, H_4, $H_{4''}$), 6.85 (d, $J_{34} = 5$ Hz, 2 H, H_3, $H_{3''}$), and 4.97 ppm (t, $J_{3'4'} = 8.5$ Hz, 1 H, $H_{4'}$).

$[(tpy)(H_2O)_2Ru^{III}ORu^{III}(H_2O)_2(tpy)]^{4+}$ (2). This complex was generated in situ by dissolution of $[(tpy)(C_2O_4)Ru^{III}ORu^{III}(C_2O_4)(tpy)]\cdot 8H_2O$ in 1 M $HClO_4$ (pH = 0). We were unable to isolate a solid form of the tetraaqua complex.[28]

$[(tpy)(CO_3)Ru^{III}ORu^{III}(CO_3)(tpy)]\cdot 7H_2O$ (3·7H$_2$O). A 0.5-g sample of $[(tpy)(C_2O_4)Ru^{III}ORu^{III}(C_2O_4)(tpy)]\cdot 8H_2O$ was dissolved in a minimum amount of 1 M $HClO_4$ to form $[(tpy)(H_2O)_2Ru^{III}ORu^{III}(H_2O)_2$-$(tpy)]^{4+}$ ($\lambda_{max} = 598$ nm). Enough Na_2CO_3 was added to the solution to neutralize the acid and precipitate the crude product. The solid that formed was filtered and washed with alkaline water. It was dissolved in a minimum amount of water and purified by column chromatography by using Sephadex LH-20 and water as the eluent. Yield after rotary evaporation: 82%. Anal. Calcd for $C_{32}H_{36}N_6O_{14}Ru_2$: C, 41.29; H, 3.90; N, 9.03. Found: C, 40.55; H, 3.97; N, 9.51.

Instrumental Measurements. Electrochemical measurements were conducted with a Princeton Applied Research model 273 potentiostat. Spectroelectrochemical experiments were performed in a three-compartment electrochemical cell in which the working electrode compartment was a 1-cm cell. Controlled-potential electrolysis experiments were carried out by using a reticulated vitreous carbon gauze electrode (60 PPI, The Electrosynthesis Co., Inc., Lancaster, NY). Cyclic voltammetric experiments were carried out in a three-compartment cell by using a glassy carbon disk working electrode, a platinum wire as the counter electrode, and a Hg/Hg_2SO_4 reference electrode. The glassy carbon working electrode was polished with 0.3-μm alumina and sonicated in distilled water immediately prior to use. The pH of solutions was determined by using an ATI Orion EA940 model pH meter and an Orion 8103 Ross combination electrode with automatic temperature compensation after calibration with standard buffers. Buffer solutions for electrochemical measurements were prepared from aqueous perchloric acid, $HClO_4$, with $LiClO_4$ (pH = 1−2), and $HClO_4$ with $NaH_2PO_4\cdot H_2O$, $Na_2HPO_4\cdot 7H_2O$, $Na_3PO_4\cdot 12H_2O$ (pH = 2−12), and NaOH with $Na_3PO_4\cdot 12H_2O$ (pH = 12−14). The $E_{1/2}$ values reported in this work were calculated from cyclic voltammetric waveforms as an average of the oxidative and reductive peak potentials, $(E_{p,a} + E_{p,c})/2$. All cyclic voltammograms were obtained after purging with argon.

Table 1. Crystallographic Data for $[(tpy)(C_2O_4)Ru^{III}ORu^{III}(C_2O_4)(tpy)]\cdot 8H_2O$[a]

formula: $C_{34}H_{38}N_6O_{17}Ru_2$	fw: 1004.83
$a = 18.950(4)$ Å	space group: monoclinic, $I\,2/a$
$b = 13.318(3)$ Å	$T = -110$ °C (163 K)
$c = 32.986(5)$ Å	$\lambda = 0.710\ 73$ Å
$\beta = 105.605(14)°$	$\mu = 0.082$ cm^{-1}
$V = 8018(3)$ Å^3	$R = 0.055$, $R_w = 0.060$
$Z = 8$	GOF = 1.43
NO = 5588	NO[$>2\sigma(I)$] = 3049
$D_{calc} = 1.665$ Mg m^{-3}	

equivalent positions: (1) x, y, z; (2) $1/2 - x, y, -z$
centering vectors: (1) 0, 0, 0; (2) $^1/_2$, $^1/_2$, $^1/_2$

[a] $R = \sum(F_o - F_c)/\sum(F_o)$, $R_w = [\sum(F_o - F_c)^2/\sum(F_o^2)]^{1/2}$, GOF = $[\sum(F_o - F_c)^2/$(no. of reflns − no. of params)$]^{1/2}$.

X-ray crystallographic analysis was performed by Dr. Peter White in the X-ray facility at the University of North Carolina. The structure of $[(tpy)(C_2O_4)Ru^{III}ORu^{III}(C_2O_4)(tpy)]\cdot 8H_2O$ was determined at −110 °C (163 K) on a Rigaku diffractometer in the ω scan mode. Crystal data and experimental parameters are tabulated in Table 1. The data were corrected for absorption. A total of 5588 unique reflections were collected, of which 3049 with $I_{net} > 2.5\sigma(I_{net})$ were used later in refining the structure. The last least squares cycle was calculated with 103 atoms and 535 parameters. The structure was refined by using least-squares methods to give the final values of $R = 0.055$, $R_w = 0.060$, and GOF = 1.43. All programs used were from the NRCVAX system.

UV−visible spectra were recorded in 1-cm, 5-mm, or 2-mm cells by using On-line Instrument Systems, Inc. modified Cary-14 or Hewlett-Packard model 8452A diode array spectrophotometers interfaced with an IBM-compatible PC. Molar extinction coefficients were determined from measurements at three or more concentrations. The temperature of solutions during kinetic studies was maintained to within ±0.2 °C with use of a Lauda RM6 circulating water bath and monitored with an Omega HH-51 thermocouple probe.

^{1}H NMR spectra were obtained in D_2O or $HClO_4$-acidified D_2O on a Bruker WM-250 MHz FT-NMR spectrometer. IR spectra were recorded on a Mattson Galaxy 5020 series FT-IR spectrophotometer interfaced with a Macintosh computer. IR measurements were made in KBr pellets.

Dioxygen detection was achieved by use of an Orion model 97-08-00 O_2 electrode interfaced to a Radiometer PHM62 standard pH meter. The electrode was mounted to sample headspace gases. The reaction chamber accepted reactants through a septum while purging gas entered and exited the chamber through stopcock fitted joints that were in the closed position during measurements. Kinetic runs were initiated by syringe-injecting the Ce^{IV} solution into the stirred solutions containing **2**. Both the cerium and solutions of **2**, as well as the reaction chamber, were purged of O_2 by bubbling with N_2 or Ar prior to mixing. Electrode response upon initiating the reaction was monitored by interfacing the pH meter to a computer with the DU stopped-flow program (model 4000 Data System, version 7.03, On-Line Instruments, Inc., Jefferson, GA). The total volume of oxygen gas produced was calculated on the basis of the volume of the headspace which was measured after the experiment and calibration of the electrode based on known values. The number of moles produced was calculated from the partial pressure of dissolved oxygen and the ideal gas law.

Resonance Raman spectra were obtained at the UNC Laser Laboratory. Samples were contained in NMR tubes and examined in a spinning arrangement. Raman scattering was collected at 135° to the incident radiation, which was supplied by the 647.1- or 442-nm lines of a Spectra-Physics 165-05 Ar^+ laser. Laser power was ca. 50 mW at the sample. Detection was achieved through use of a Princeton Applied Instruments model ICCD and WinSpec software (version 1.6.1).

(24) Sullivan, B. P.; Calvert, J. M.; Meyer, T. J. *Inorg. Chem.* **1980**, *19*, 1404−1407.
(25) Dovletoglou, A.; Adeyemi, S. A.; Lynn, M. H.; Hodgson, D. J.; Meyer, T. J. *J. Am. Chem. Soc.* **1990**, *112*, 8989−8990.
(26) Adeyemi, S. A.; Dovletoglou, A.; Guadalupe, A. R.; Meyer, T. J. *Inorg. Chem.* **1992**, *31*, 1375−1383.
(27) Dovletoglou, A. Ph.D. Dissertation. University of North Carolina, Chapel Hill, 1992.
(28) Attempts at precipitation were made with the counterions: tetrafluoroborate, hexafluorophosphate, triflate, perchlorate, tetrakis(3,5-bis-(trifluoromethyl)phenyl)borate, mesitylene-2-sulfonate, nitrate, and *p*-toluenesulfonate.

Scheme 1

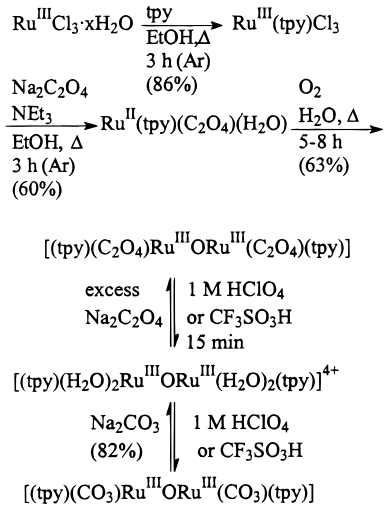

Results

The complexes $[(tpy)(C_2O_4)Ru^{III}ORu^{III}(C_2O_4)(tpy)]\cdot 8H_2O$ (**1**·$8H_2O$) and $[(tpy)(CO_3)Ru^{III}ORu^{III}(CO_3)(tpy)]\cdot 7H_2O$ (**3**·$7H_2O$) were used as precursors to $[(tpy)(H_2O)_2Ru^{III}ORu^{III}(H_2O)_2(tpy)]^{4+}$ (**2**). Their preparations are outlined in Scheme 1.

In cyclic voltammograms of **1**·$8H_2O$, a pH-independent $Ru^{IV}ORu^{III}/Ru^{III}ORu^{III}$ couple appears at $E_{1/2} = 0.73$ V vs NHE[29] in the range pH = 4−8 and a single, $Ru^{III}ORu^{III}$ to $Ru^{II}ORu^{II}$ two-electron reduction appears at 0.24 V at pH = 4.0. $E_{1/2}$ for this wave decreases with a slope of 30 mV per pH unit between pH 4 and 8, consistent with the two-electron/one-proton couple in eq 1. On the longer time scale for controlled potential electrolysis ($E_{app} = 0$ at pH = 8, $n = 2.0 \pm 0.1$), reductive cleavage occurs to give $Ru^{II}(tpy)(C_2O_4)(OH_2)$, as shown by UV−vis spectral comparisons.

$$(tpy)(C_2O_4)Ru^{III}ORu^{III}(tpy)(C_2O_4) + 2e^- + H^+ \rightarrow (tpy)(C_2O_4)Ru^{II}(OH)Ru^{II}(tpy)(C_2O_4)^- \quad (1)$$

$$(tpy)(C_2O_4)Ru^{II}(OH)Ru^{II}(tpy)(C_2O_4)^- + 2H_2O \rightarrow 2(tpy)(C_2O_4)Ru^{II}(OH_2) + OH^- \quad (2)$$

In the structure of **1** in Figure 1, the coordination geometry at each Ru(III) is a slightly distorted octahedron composed of a meridionally bound terpyridyl ligand, a bidentate oxalate ligand, and a bridging oxo ligand. The tpy ligands of the two Ru ions are stacked in a slightly staggered configuration with a torsional angle of 22.7°. The RuORu angle is 148.5°. The Ru−O average bond distance of 1.843 Å for the oxo bridge suggests Ru−O multiple bonding in the RuORu core. The average $Ru-O_{ox}$ distance of 2.091 Å is consistent with Ru−O single bonding. The Ru−O bond lengths of the oxalate oxygens *trans* to the bridge are significantly shorter (2.080 and 2.067 Å) than the Ru−O bond lengths of the oxygens in the *cis* positions (both 2.108 Å). The angles between the *trans*-N atoms in the tpy ligand and the Ru atoms are considerably less than 180° (159.1° and 159.3°). Selected bond distances and angles are presented in Table 2. A complete description of parameters, structure solution and refinement conditions, atomic coordinates, bond distances and angles, and thermal parameters is provided as Supporting Information.

Both **1**·$8H_2O$ and **3**·$7H_2O$ undergo acid hydrolysis in 1 M $HClO_4$ or CF_3SO_3H to give $[(tpy)(H_2O)_2Ru^{III}ORu^{III}(H_2O)_2(tpy)]^{4+}$ (**2**) within minutes. For **1**, the reaction is accompanied by a shift in λ_{max} from 636 to 598 nm. Aquation of **1** is complete in ∼2 h at pH = 1 and takes many hours at pH = 2. **1** is stable indefinitely between pH = 4 and 8, but at pH = 13 it undergoes loss of oxalate and air-oxidation to give $[(tpy)(OH)_2Ru^{III}ORu^{IV}(H_2O)(OH)(tpy)]^{2+}$ within 10 min.

We have been unable to isolate a solid form of $[(tpy)(H_2O)_2Ru^{III}ORu^{III}(H_2O)_2(tpy)]^{4+}$.[30] The RuORu core is retained as shown by UV−visible and resonance Raman spectra (see below) and by precipitation as the carbonate dimer, **3**, by addition of excess sodium carbonate. Redissolution of **3**·$7H_2O$ in acid gives back **2** quantitatively, as shown by electrochemical and spectral measurements.

In the ^1H NMR spectrum of **2** in the terpyridine region in $HClO_4$-acidified D_2O, tpy resonances appear at 7.83 ppm (d, $J_{56} = 8$ Hz, 2 H, H_6, $H_{6''}$), 7.45 ppm (ddd, $J_{45} = 7.62$ Hz, $J_{34} = 7.75$ Hz, $J_{46} = 1.75$ Hz, 2 H, H_4, $H_{4''}$), 7.31 ppm (d, $J_{34} = 7.75$ Hz, 2 H, H_3, $H_{3''}$), 7.08 ppm (multiplet, 4 H, H_5, $H_{5''}$, $H_{3'}$, $H_{5'}$), and 5.64 ppm (t, $J_{3'4'} = 8$ Hz, 1 H, $H_{4'}$). The spectrum of $[(tpy)(H_2O)_2Ru^{III}ORu^{IV}(H_2O)_2(tpy)]^{5+}$ is paramagnetically broadened into the base line. In the resonance Raman spectrum of $[(tpy)(H_2O)_2Ru^{III}ORu^{III}(H_2O)_2(tpy)]^{4+}$ (647.1-nm excitation, 1 M $HClO_4$), ν_{sym}(RuORu) appears as an intense band at 474 cm^{-1} [16] but the asymmetric stretch at higher energy is of low intensity and not discernible. Summaries of IR and resonance Raman data for $[(tpy)(C_2O_4)Ru^{III}ORu^{III}(C_2O_4)(tpy)]$, $[(tpy)(H_2O)_2Ru^{III}ORu^{III}(H_2O)_2(tpy)]^{4+}$, and $[(tpy)(H_2O)_2Ru^{IV}ORu^{III}(H_2O)_2(tpy)]^{5+}$ are given elsewhere.[31] UV−visible spectra for the $Ru^{III}ORu^{III}$, $Ru^{IV}ORu^{III}$, and $Ru^{IV}ORu^{IV}$ forms of **2** at pH 1 (Supporting Information) are summarized in Table 3. The spectrum of $Ru^{III}ORu^{III}$ is pH dependent because of the acidity of the bound waters and the equilibria in eqs 3 and 4. pK_a values were determined by spectrophotometric titration and are listed in Table 4. For $Ru^{IV}ORu^{III}$, $\lambda_{max} = 472$ nm for $[(tpy)(H_2O)_2Ru^{III}ORu^{III}(H_2O)_2(tpy)]^{4+}$

$$[(tpy)(H_2O)_2Ru^{III}ORu^{III}(H_2O)_2(tpy)]^{4+} \rightleftharpoons H^+ + [(tpy)(H_2O)(OH)Ru^{III}ORu^{III}(H_2O)_2(tpy)]^{3+} \quad pK_{a_1} = 4.4 \quad (3)$$

$$[(tpy)(H_2O)(OH)Ru^{III}ORu^{III}(H_2O)_2(tpy)]^{3+} \rightleftharpoons H^+ + [(tpy)(H_2O)(OH)Ru^{III}ORu^{III}(H_2O)(OH)(tpy)]^{2+} \quad pK_{a_2} = 10.5 \quad (4)$$

$Ru^{IV}ORu^{III}(H_2O)(OH)(tpy)]^{4+}$, $\lambda_{max} = 500$ nm for $[(tpy)(H_2O)(OH)Ru^{IV}ORu^{III}(H_2O)(OH)(tpy)]^{3+}$, and $\lambda_{max} = 512$ nm with a new band appearing at 394 nm for $[(tpy)(OH)_2Ru^{IV}ORu^{III}(OH)(OH_2)(tpy)]^{2+}$. From spectrophotometric titrations, $pK_{a_2} \approx 3.7$ and $pK_{a_3} \approx 9.4$ at 22 °C (Table 4).

Solutions containing $[(tpy)(H_2O)_2Ru^{IV}ORu^{IV}(H_2O)(OH)(tpy)]^{5+}$ (**5**) were prepared by controlled potential oxidation of **2** at 0.50 V (vs Hg/Hg_2SO_4, 1.14 V vs NHE, pH = 0, $n = 2.1 \pm 0.1$). The pK_a values in Table 5 are estimates from the

(29) Cyclic voltammograms and controlled-potential electrolyses were referenced to the Hg/Hg_2SO_4 couple. NHE = Hg/Hg_2SO_4 + 640 mV = SCE + 241 mV. Potentials reported in this paper are referenced to NHE.

(30) Oligomerization is a complication in concentrated solutions. One product is $[(tpy)(H_2O)_2Ru^{III}ORu^{IV}(tpy)(H_2O)ORu^{III}(tpy)(H_2O)_2]^{5+}$, which has been prepared independently by addition of $[(tpy)(ox)Ru^{III}ORu^{IV}(tpy)(H_2O)ORu^{III}(tpy)(ox)]^{2+}$ to 1 M acid. (Dovletoglou, A. Ph.D. Dissertation. University of North Carolina, Chapel Hill, 1992.)

(31) Lebeau, E. L. Ph.D. Dissertation. University of North Carolina, Chapel Hill, 1997.

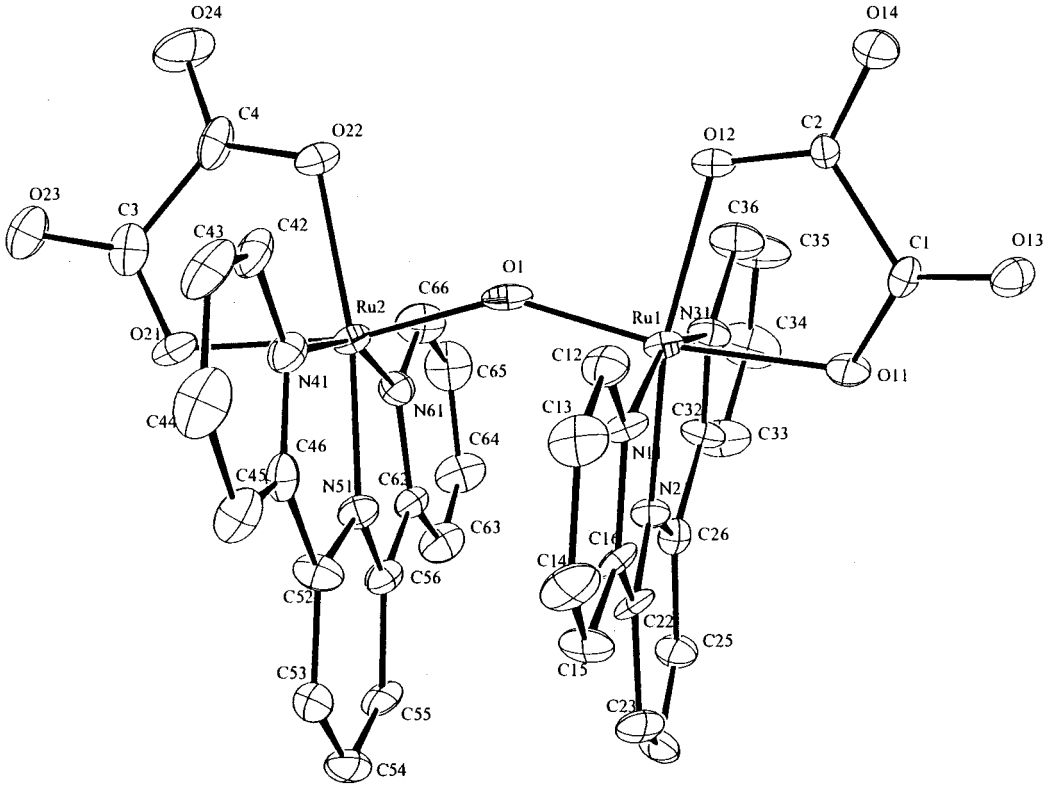

Figure 1. ORTEP drawing of $[(tpy)(C_2O_4)Ru^{III}ORu^{III}(tpy)(C_2O_4)]\cdot 8H_2O$, $\mathbf{1}\cdot 8H_2O$.

Table 2. Selected Bond Distances (Å) and Angles (deg) for $[(tpy)(C_2O_4)Ru^{III}ORu^{III}(C_2O_4)(tpy)]\cdot 8H_2O$ Based on the Labeling Scheme in Figure 1

Ru(1)−O(1)	1.841(8)	Ru(2)−O(1)	1.846(8)
Ru(1)−O(11)	2.067(8)	Ru(2)−O(21)	2.080(9)
Ru(1)−O(12)	2.108(7)	Ru(2)−O(22)	2.108(8)
Ru(1)−N(11)	2.058(9)	Ru(2)−N(41)	2.076(10)
Ru(1)−N(21)	1.950(9)	Ru(2)−N(51)	1.930(10)
Ru(1)−N(31)	2.093(10)	Ru(2)−N(61)	2.076(10)
O(1)−Ru(1)−O(11)	169.5(3)	O(1)−Ru(2)−O(21)	168.1(3)
O(1)−Ru(1)−O(12)	90.8(3)	O(1)−Ru(2)−O(22)	88.7(3)
O(1)−Ru(1)−N(11)	94.6(3)	O(1)−Ru(2)−N(41)	94.8(3)
O(1)−Ru(1)−N(21)	99.5(4)	O(1)−Ru(2)−N(51)	100.5(4)
O(1)−Ru(1)−N(31)	93.9(4)	O(1)−Ru(2)−N(61)	93.5(4)
O(11)−Ru(1)−O(12)	79.0(3)	O(21)−Ru(2)−O(22)	79.4(3)
O(11)−Ru(1)−N(11)	84.7(3)	O(21)−Ru(2)−N(41)	87.0(4)
O(11)−Ru(1)−N(21)	90.7(4)	O(21)−Ru(2)−N(51)	91.4(4)
O(11)−Ru(1)−N(31)	90.4(4)	O(21)−Ru(2)−N(61)	88.8(4)
O(12)−Ru(1)−N(11)	100.0(3)	O(22)−Ru(2)−N(41)	100.8(4)
O(12)−Ru(1)−N(21)	169.7(4)	O(22)−Ru(2)−N(51)	170.7(4)
O(12)−Ru(1)−N(31)	99.0(3)	O(22)−Ru(2)−N(61)	98.3(4)
N(11)−Ru(1)−N(21)	80.0(4)	N(41)−Ru(2)−N51)	79.9(4)
N(11)−Ru(1)−N(31)	159.1(4)	N(41)−Ru(2)−N(61)	159.3(4)
N(21)−Ru(1)−N(31)	79.7(4)	N(51)−Ru(2)−N(61)	80.0(4)
Ru(1)−O(1)−Ru(2)	148.5(4)		

breakpoints in $E_{1/2}$−pH plots from electrochemical measurements, see below. Attempts to record resonance Raman spectra were unsuccessful due to photoreduction (and oxygen evolution). This chemistry is currently under investigation.

Redox Chemistry. Cyclic voltammograms of **2** at glassy carbon electrodes in water provide evidence for a variety of pH-dependent redox processes (Supporting Information). In 1 M $HClO_4$ under Ar, the following features appear: (1) Two overlapping, irreversible one-electron reductions at $E_{p,c} = 0.27$ and 0.19 V vs NHE ($n = 2.0 \pm 0.2$ by coulometry at $E_{app} = -0.55$ V). Controlled-potential electrolysis past either wave results in reductive cleavage to give $[Ru^{II}(tpy)(OH_2)_3]^{2+}$, as shown by the appearance of waves at $E_{1/2} = 0.71$ V vs NHE at pH = 1 for the $Ru^{III/II}$ couple of the product and $\lambda_{max} = 532$ nm ($\epsilon = 3450\ M^{-1}\ cm^{-1}$).[8,9] The same product is obtained by reduction with ascorbic acid in excess. (2) Distinct one-electron oxidation waves (by peak current comparison) at 0.91 and 1.04 V vs NHE arising from $Ru^{IV}ORu^{III}/Ru^{III}ORu^{III}$ and $Ru^{IV}ORu^{IV}/Ru^{IV}ORu^{III}$ couples. From controlled-potential electrolysis, $n = 1.1 \pm 0.1$ at $E_{app} = 0.94$ V and 1.0 ± 0.2 at $E_{app} = 1.29$ V (vs NHE). (3) An irreversible, seemingly multielectron wave at $E_{p,a} = 1.56$ V, which results in $[Ru^{VI}(tpy)(O)_2(OH_2)]^{2+}$, see below.

The features that appear in the cyclic voltammogram at pH = 5.65 are as follows: (1) a single, two-electron, chemically reversible reduction at 0.14 V; (2) the $Ru^{IV}ORu^{III}/Ru^{III}ORu^{III}$ and $Ru^{IV}ORu^{IV}/Ru^{IV}ORu^{III}$ couples at −0.47 and 0.73 V vs NHE ($n = 1.0 \pm 0.1$ at $E_{app} = 0.55$ V and 1.1 ± 0.2 at $E_{app} = 0.8$ V); (3) an additional, apparently one-electron oxidation wave, based on relative peak currents, at 1.14 V. Measurements at higher potentials are obscured by the background at this pH.

The results of an extensive pH-dependence study are illustrated in the $E_{1/2}$−pH diagram in Figure 2. For convenience, the oxidation states are labeled as V-V for $Ru^{V}ORu^{V}$ etc. The vertical dashed lines represent the pK_a values of the corresponding complexes as determined by spectrophotometric titrations or inferred from $E_{1/2}$−pH data. The lines drawn through the experimental points have slopes of 0, −30, −60, or −120 mV per pH unit as predicted by the Nernst equation in the form $E^{\circ\prime} = E_{1/2} - 0.05916(m/n)$(pH) with m the number of protons, n the number of electrons, and $E_{1/2}$ the half-wave potential at pH = 0.[32] Analysis of the data and the conclusions reached in Figure 2 follow from refs 12 and 16.

In interpreting this diagram, abbreviations such as $(OH_2)_3(OH)/(OH_2)_4$ for the IV-III/III-III couple below pH 3.7 are used. They refer to half-reactions such as

(32) Bard, A. J.; Faulkner, L. R. *Electrochemical Methods*; John Wiley: New York, 1980.

Table 3. UV−Visible Spectral Data in H_2O at 25 °C

complex	pH	λ_{max}, nm (ϵ_{max}, L mol^{-1} cm^{-1})
$[(tpy)(C_2O_4)Ru^{III}(O)Ru^{III}(C_2O_4)(tpy)]$	7	1355 (500), 913 sh, 636 (10 500), 320 (25 200), 274 (36 200)
$[(tpy)(H_2O)_2Ru^{III}ORu^{III}(H_2O)_2(tpy)]^{4+}$	1	1287 (300), 900 sh, 598 (10 000), 568 sh, 505 sh, 455 sh, 334 sh, 324 (24 500), 272 (30 000)
$[(tpy)(H_2O)_2Ru^{III}ORu^{III}(H_2O)(OH)(tpy)]^{3+}$	6	596 (5600), 316 (19 500), 274 (22 500)
$[(tpy)(H_2O)(OH)Ru^{III}ORu^{III}(H_2O)(OH)(tpy)]^{2+}$	13	672 (5800), 573 (5000), 404 (5800), 317 (23 100), 275 (22 500)
$[(tpy)(H_2O)_2Ru^{III}ORu^{IV}(H_2O)(OH)(tpy)]^{4+}$	1	1202 (300), 688 sh, 597 sh, 472 (16 700), 364 sh, 334 sh, 320 (24,600)
$[(tpy)(H_2O)_2Ru^{IV}ORu^{IV}(H_2O)(OH)(tpy)]^{5+}$	1	1199 (400), 617 br sh, 460 (15 200), 380 (11 800), 333 sh, 322 (23 500)

Table 4. Acid Dissociation Constants in Aqueous Solution at 22 °C

acid form	p$K_{a_{hb}}$[a]	pK_{a_1}	pK_{a_2}	pK_{a_3}	pK_{a_4}
$[(tpy)(H_2O)_2Ru^{II}(OH)Ru^{II}(H_2O)_2(tpy)]^{2+}$	<4.0[b]	9.4[b]			
$[(tpy)(H_2O)_2Ru^{III}ORu^{III}(H_2O)_2(tpy)]^{4+}$		4.4[c]	10.3[c]		
$[(tpy)(H_2O)_2Ru^{III}ORu^{IV}(H_2O)_2(tpy)]^{5+}$		<0	3.7[c]	9.4[c]	
$[(tpy)(H_2O)_2Ru^{IV}ORu^{IV}(H_2O)_2(tpy)]^{6+}$		<0	2.2[b]	3.0[b]	9.8[b]

[a] Proton loss from the μ-hydroxo group. [b] From the breaks in $E_{1/2}$−pH plots, Figure 4. [c] By spectrophotometric titration; ±0.2.

Table 5. Oxygen Production by $[(tpy)(H_2O)_2Ru^{III}(O)Ru^{III}(H_2O)_2(tpy)]^{4+}$ with Added Ce(IV) in Acid Solution at 25 °C

expt	medium	mol of dimer	[dimer], M	mol of Ce(IV)	mol of O_2	efficiency[d], %	O_2/dimer
A	0.1 M $HClO_4$	4.45×10^{-6}	2.20×10^{-3}	2.72×10^{-4}	$3.87 (\pm 1.11) \times 10^{-6}$	5.7 (±1.6)	0.87 (±0.25)
B	0.1 M $HClO_4$	5.97×10^{-6}	3.14×10^{-3}	8.47×10^{-5}	$1.62 (\pm 0.66) \times 10^{-6}$	7.7 (±3.1)	0.27 (±0.11)
C	0.1 M $HClO_4$	4.88×10^{-6}	2.03×10^{-3}	3.09×10^{-4}	$3.22 (\pm 1.15) \times 10^{-6}$	4.2 (±1.4)	0.66 (±0.24)[a]
D	0.1 M $HClO_4$	2.19×10^{-6}	1.09×10^{-3}	8.47×10^{-6}	$1.62 (\pm 0.59) \times 10^{-6}$	76.5 (±15.1)	0.74 (±0.15)
E	0.1 M $HClO_4$	2.19×10^{-6}	1.02×10^{-3}	1.66×10^{-5}	$1.86 (\pm 0.71) \times 10^{-6}$	44.8 (±17.2)	0.85 (±0.32)
F	0.1 M HOTf	3.41×10^{-6}	1.55×10^{-3}	1.26×10^{-5}	$2.76 (\pm 0.88) \times 10^{-6}$	88.2 (±27.8)	0.81 (±0.26)
G	0.1 M HOTf	3.41×10^{-6}	1.42×10^{-3}	2.51×10^{-5}	$2.98 (\pm 0.92) \times 10^{-6}$	47.4 (±14.8)	0.87 (±0.27)
H	0.1 M HOTf	4.62×10^{-6}	2.15×10^{-3}	1.77×10^{-5}	$1.08 (\pm 0.62) \times 10^{-6}$	23.1 (±1.3)	0.24 (±0.14)[a]
I	2.0 M $HClO_4$	2.22×10^{-6}	1.01×10^{-3}	1.07×10^{-5}	$8.65 (\pm 4.56) \times 10^{-7}$	32.4 (±17)	0.39 (±0.20)
J	1.0 M $HClO_4$	2.91×10^{-6}	1.32×10^{-3}	7.90×10^{-6}	$1.74 (\pm 0.64) \times 10^{-6}$	88 (±32)	0.60 (±0.22)
K	0.1 M $HClO_4$	2.13×10^{-6}	9.68×10^{-4}	1.00×10^{-5}	$1.34 (\pm 0.55) \times 10^{-6}$	53.2 (±22.5)	0.63 (±0.25)
L	0.1 M $HClO_4$	2.14×10^{-6}	9.73×10^{-4}	1.73×10^{-6}	$1.82 (\pm 0.66) \times 10^{-6}$	104 (±35)	0.85 (±0.29)[b]
M	0.1 M $HClO_4$	2.87×10^{-6}	1.22×10^{-4}	2.86×10^{-4}	$3.01 (\pm 0.72) \times 10^{-6}$	4.21 (±0.87)	1.05 (±0.26)[c]
N	1.0 M $HClO_4$	2.73×10^{-6}	1.20×10^{-4}	1.56×10^{-5}	$1.24 (\pm 0.54) \times 10^{-6}$	32 (±9.9)	0.46 (±0.19)
O	1.0 M $HClO_4$	2.73×10^{-6}	1.15×10^{-4}	3.36×10^{-6}	$2.11 (\pm 0.50) \times 10^{-6}$	62.8 (±5.4)	0.77 (±0.14)[b]

[a] At 5 °C. [b] By addition to $Ru^{IV}-O-Ru^{IV}$ generated by electrolysis. [c] Under dilute conditions with [**2**] < 1.5×10^{-4} M. [d] Percentage Ce^{IV} generating O_2.

$$[(tpy)(H_2O)(OH)Ru^{IV}ORu^{III}(H_2O)_2(tpy)]^{4+} + e^- + H^+ \rightleftharpoons [(tpy)(H_2O)_2Ru^{III}ORu^{III}(H_2O)_2(tpy)]^{4+} \quad (5)$$

Protonation of II−II as $[(tpy)(H_2O)_2Ru^{II}ORu^{II}(H_2O)_2(tpy)]^{2+}$ at pH < 4 presumably occurs at the μ-oxo bridge to give $[(tpy)(H_2O)_2Ru^{II}(OH)Ru^{II}(H_2O)_2(tpy)]^{3+}$. Assignment of proton structures to forms in which more than one proton is lost is somewhat arbitrary. For example, for $Ru^{III}ORu^{IV}$ above pH = 9.4, the structure could be $[(tpy)(H_2O)(OH)Ru^{IV}ORu^{III}(H_2O)(OH)(tpy)]^{3+}$, $[(tpy)(H_2O)(O)Ru^{IV}ORu^{IV}(H_2O)_2(tpy)]^{3+}$, or even $[(tpy)(OH)_2Ru^{IV}ORu^{III}(H_2O)_2(tpy)]^{3+}$. Oxidation state $Ru^{IV}ORu^{IV}$ could be either $Ru^{IV}ORu^{IV}$ or $Ru^{V}ORu^{III}$. The distribution $Ru^{V}ORu^{III}$ is known to exist in $[(bpy)_2(O)Ru^{V}ORu^{III}(py)(bpy)_2]^{4+}$.[33] It is assumed that terminal oxo formation is important for oxidation past Ru^{IV} in order to stabilize the higher oxidation states. With this assumption, the dominant form of $Ru^{V}ORu^{IV}$ would be $[(tpy)(H_2O)(O)Ru^{V}ORu^{IV}(O)(H_2O)(tpy)]^{3+}$ below pH 9.8 and $[(tpy)(OH)(O)Ru^{V}ORu^{IV}(O)(H_2O)(tpy)]^{2+}$ above pH 9.8, for example.

From pH = 2 to 8.5 there is evidence for an additional one-electron oxidation, presumably from $Ru^{V}ORu^{IV}$ to $Ru^{V}ORu^{V}$. This wave is pH independent and chemically irreversible with $E_{p,a} \approx 1.44$ V vs NHE [$E_{1/2} \approx (0.845/n)E_{p,a} = 1.22$ V, assuming applicability of the Cottrell equation].[33] Oxidation past this wave results in rapid decomposition and the appearance, on the reverse scan, of waves for couples associated with *trans*-$[Ru^{VI}(tpy)(O)_2(H_2O)]^{2+}$ ($E_{1/2}$ = 1.27, 1.11, and 0.71 V vs NHE at pH = 1).[9]

In solutions more acidic than pH 4, a single, irreversible, multielectron oxidation wave is observed, presumably arising from the $Ru^{V}ORu^{V}/Ru^{IV}ORu^{IV}$ couple. By comparison, for the blue dimer at pH 2, a reversible three-electron oxidation occurs at ~1.29 V vs NHE for the $Ru^{V}ORu^{V}/Ru^{IV}ORu^{III}$ couple. Oxidative scans past this wave result in decomposition and the appearance of waves characteristic of *trans*-$[Ru^{VI}(tpy)(O)_2(H_2O)]^{2+}$. Controlled-potential electrolysis of solutions containing $Ru^{IV}ORu^{IV}$ at E_{app} > 1.64 V vs NHE occurs with n > 5, cleavage of the μ-oxo structure, and quantitative formation of $[Ru^{VI}(tpy)(O)_2(OH_2)]^{2+}$ as determined by spectrophotometric comparison with an authentic sample [λ_{max}, nm (ϵ, M^{-1} cm^{-1}) = 410 (3700) at pH = 1].[8,9] Controlled-potential electrolysis is complicated and accompanied by decomposition, water oxidation, and catalytic oxidation of the glassy carbon working electrode.

Reactivity Studies and Oxygen Evolution. With **2** in acidic solution, addition of Ce^{IV} results in the production of dioxygen. In Table 5 are shown the results of a series of oxygen evolution experiments carried out in triflic and perchloric acid solutions. The chemistry is complex, but a series of conclusions can be reached from the data: (1) By inference, the catalyst is deactivated after 1 turnover through the catalytic cycle since the maximum number of moles of oxygen produced per mole of **2** approaches, but does not exceed, 1 within experimental

(33) Doppelt, P.; Meyer, T. J. *Inorg. Chem.* **1987**, *26*, 2027−2034.

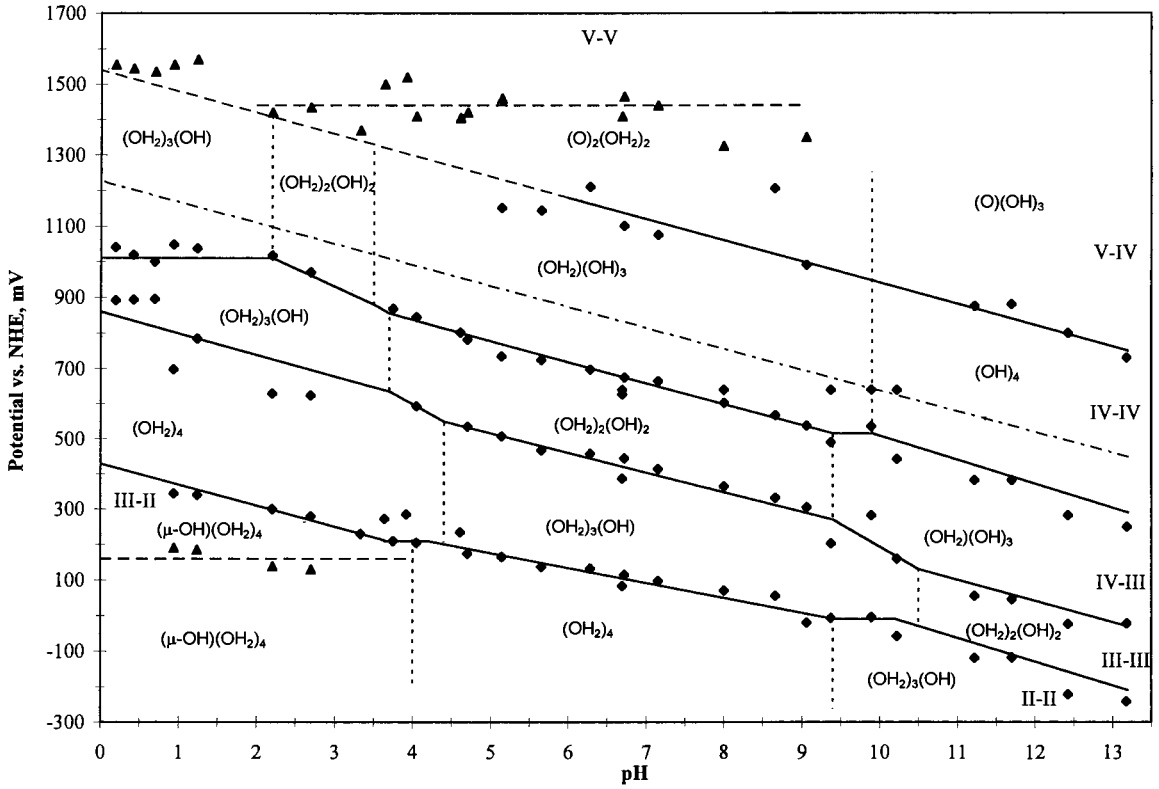

Figure 2. pH dependence of $E_{1/2}$ values for the redox couples of $[(tpy)(H_2O)_2Ru^{III}ORu^{III}(H_2O)_2(tpy)]^{4+}$, $\mu = 0.1$ M. Proton compositions are indicated; for example, III/III $(OH_2)_4$ is a representation for $[(tpy)(H_2O)_2Ru^{III}ORu^{III}(H_2O)_2(tpy)]^{4+}$. Vertical lines (- - -) are drawn from the breaks in the $E_{1/2}$ values and represent pK_a values determined by spectrophotometric titration or inferred from the $E_{1/2}$−pH data. The potential−pH regions where the various oxidation states are dominant are indicated in the diagram. The dashed diagonal line (−•−•) is the potential for the oxygen/water couple as a function of pH. The dashed lines (− − −) indicate regions where $E_{p,a}$ or $E_{p,c}$ values are cited rather than $E_{1/2}$ due to chemical irreversibility. The assignment of oxidation states in the mixed-valence forms and of proton structure in the multiple proton loss forms is somewhat arbitrary; see text.

error. (2) The efficiency of O_2 evolution (per Ce^{IV} added) increases in proportion to the amount of complex present.

To gain insight into the water oxidation mechanism, a series of mixing experiments were performed with spectrophotometric monitoring. The first series of experiments involved mixing a concentrated solution of **2** (1×10^{-2} to 5×10^{-3} M) with an excess (greater than 13 equiv) of Ce^{IV} in 2 M perchloric acid. The final product was $[Ru^{VI}(tpy)(O)_2(OH_2)]^{2+}$ ($\lambda_{max} = 410$ nm, $\epsilon = 3700$ M^{-1} cm^{-1}),[8,9] which precipitates from solution as the perchlorate salt under these conditions.

In solutions of $Ru^{IV}ORu^{IV}$ generated by electrolysis, subsequent addition of a large excess of Ce^{IV}(>10 equiv) resulted in the quantitative formation of $[Ru^{VI}(tpy)(O)_2(OH_2)]^{2+}$. Addition of 1 or 2 equiv of Ce^{IV} resulted in complex spectral changes. The product solution contained $[Ru^{VI}(tpy)(O)_2(OH_2)]^{2+}$ and a new $Ru^{IV}ORu^{IV}$ species, $Ru^{IV}ORu^{IV\prime}$, with $\lambda_{max} = 376$ and 447 nm rather than 380 and 460 nm. In cyclic voltammograms at 10 mV/s at 10° in 1 M perchloric acid, $Ru^{IV}ORu^{IV\prime}$ has waves at $E_{1/2} = 1.02$, 0.82, and 0.36 V vs NHE compared to 1.01, 0.86, and 0.43 V for $Ru^{IV}ORu^{IV}$ generated electrolytically. The differences are reproducible. $Ru^{IV}ORu^{IV\prime}$ does not undergo further oxidation. Reduction of $Ru^{IV}ORu^{IV\prime}$ with Fe^{II} gave back the spectrum of $[(tpy)(H_2O)_2Ru^{III}ORu^{III}(H_2O)_2(tpy)]^{4+}$ after several minutes, consistent with retention of the basic Ru−O−Ru core.

The effect of varying the initial $Ru^{IV}ORu^{IV}$concentration from 1.2 to 3.4×10^{-4} M on the final $Ru^{IV}ORu^{IV\prime}$:$[Ru^{VI}(tpy)(O)_2(OH_2)]^{2+}$ ratio was investigated. Ce^{IV} was added in a ×2 excess, and the product distribution was determined spectrophotometrically. The product ratio varied from 4:1 at $[Ru^{IV}ORu^{IV}] = 1.2 \times 10^{-4}$ M to ~2:1 at $[Ru^{IV}ORu^{IV}] = 3.4 \times 10^{-4}$ M. From the data in Table 5, the efficiency of oxygen production per Ce^{IV} added also increases with dimer concentration under these conditions.

Spectra of $[(tpy)(H_2O)_2Ru^{III}ORu^{III}(H_2O)_2(tpy)]^{4+}$ with 2 and 5 equiv of Ce^{IV} added were recorded on the 0.1-s time scale by rapid-scan, stopped-flow spectrophotometry (Supporting Information). Salient features include the following: (1) Even with ×5 Ce^{IV}, oxidation past $Ru^{IV}ORu^{III}$ is not observed. (2) With ×2 Ce^{IV}, the final spectrum includes some $[(tpy)(H_2O)_2Ru^{III}ORu^{III}(H_2O)_2(tpy)]^{4+}$, as evidenced by the absorption feature at $\lambda_{max} = 600$ nm.

Dimerization and Oligomerization. The redox properties of $[Ru^{II}(tpy)(H_2O)_3]^{2+}$ and its oxidation to Ru^{III}, Ru^{IV}, and Ru^{VI} were reported previously.[8,9] Reduction of $[Ru^{VI}(tpy)(O)_2(OH_2)]^{2+}$ by Fe^{II} was followed by stopped-flow, rapid-scan spectrophotometry. With $[Fe^{II}]$ (as $Fe^{II}SO_4 \cdot 7H_2O$) from 1.4 to 7×10^{-4} M and $[Ru^{VI}(tpy)(O)_2(OH_2)]^{2+} = 1.4 \times 10^{-4}$ M in 1 M $HClO_4$, reduction occurs on the mixing time of the apparatus (~2 ms). Addition of 1 equiv of Fe^{II} gave a mixture of unreacted $[Ru^{VI}(tpy)(O)_2(OH_2)]^{2+}$ and $[(tpy)(H_2O)_2Ru^{IV}ORu^{IV}(OH)(H_2O)(tpy)]^{5+}$. Addition of 2 equiv of Fe^{II} gave $[(tpy)(H_2O)_2Ru^{IV}ORu^{IV}(OH)(H_2O)(tpy)]^{5+}$ quantitatively. There was no evidence for intermediate oxidation states, in particular for a Ru^{IV} monomer. Addition of further equivalents of Fe^{II} gave mixtures of $[(tpy)(H_2O)_2Ru^{III}ORu^{III}(H_2O)_2(tpy)]^{4+}$, $[(tpy)(H_2O)(HO)Ru^{IV}ORu^{III}(H_2O)_2(tpy)]^{4+}$, and unreacted $[(tpy)(H_2O)_2Ru^{IV}ORu^{IV}(H_2O)(OH)(tpy)]^{5+}$ on the time scale of mixing. Addition of an excess of Fe^{II} (>10 equiv) led to reduction to $[(tpy)(H_2O)_2$-

$Ru^{III}ORu^{III}(H_2O)_2(tpy)]^{4+}$ (~2−3 s), followed by slower (~60 s) reductive cleavage of $Ru^{III}ORu^{III}$ to $[Ru^{II}(tpy)(H_2O)_3]^{2+}$.

These observations are consistent with initial reduction of Ru^{VI} to Ru^{V} followed by rapid reduction of Ru^{V} to Ru^{IV} and dimerization,

$$[Ru^{VI}(tpy)(O)_2(OH_2)]^{2+} + Fe^{II} \rightarrow Ru^{V} + Fe^{III} \quad (6)$$

$$Ru^{V} + Fe^{II} \rightarrow [Ru^{IV}(tpy)(OH_2)_2(O)]^{2+} + Fe^{III} \quad (7)$$

$$2\,[Ru^{IV}(tpy)(OH_2)_2(O)]^{2+} \rightarrow Ru^{IV}ORu^{IV} \quad \text{(very rapid)} \quad (8)$$

A corresponding chemistry exists in the oxidation of $[Ru^{III}(tpy)(OH_2)_3]^{3+}$ by Ce^{IV} although complications exist from water oxidation once dimers form. Addition of 1 equiv of Ce^{IV} results in quantitative oxidation of Ru^{II} to Ru^{III}. Addition of further equivalents causes oxidation of Ru^{III} to Ru^{IV}, followed by dimerization. These observations are consistent with

$$[Ru^{II}(tpy)(H_2O)_3]^{2+} + Ce^{IV} \rightarrow [Ru^{III}(tpy)(H_2O)_3]^{3+} + Ce^{III} \quad (9)$$

$$[Ru^{III}(tpy)(H_2O)_3]^{3+} + Ce^{IV} \rightarrow Ru^{IV} + Ce^{III} \quad (10)$$

$$2Ru^{IV} \rightarrow Ru^{IV}ORu^{IV} \quad \text{(very rapid)} \quad (11)$$

Evidence for higher oligomers is also obtained with Ce^{IV} oxidation at high initial concentrations of **2**. The additional product or products form in small amounts with $\lambda_{max} > 600$ nm. One product is $[(tpy)(H_2O)_2Ru^{III}ORu^{IV}(tpy)(H_2O)ORu^{III}(H_2O)_2(tpy)]^{6+}$ [$\lambda_{max} = 702$ nm ($\epsilon = 50\,100$ M^{-1} cm^{-1}) at pH = 1].[31]

Simple mixing experiments with spectrophotometric monitoring reveal that reaction between $[Ru^{VI}(tpy)(O)_2(OH_2)]^{2+}$ and $[(tpy)(H_2O)_2Ru^{III}ORu^{III}(H_2O)_2(tpy)]^{4+}$ gives $Ru^{IV}ORu^{III}$, $Ru^{IV}ORu^{IV}$, and some oligomer (<15% as estimated spectrophotometrically). Similarly, mixing reactions between $[Ru^{VI}(O)_2(OH_2)(tpy)]^{2+}$ and $Ru^{III}ORu^{IV}$ give $Ru^{IV}ORu^{IV}$ and oligomers. Oligomers form when solutions containing either $Ru^{III}ORu^{III}$ or $Ru^{IV}ORu^{III}$ are concentrated in attempts to prepare solid products.

At very high Ce^{IV} (>1×10^{-2} M), $[Ru^{VI}(tpy)(O)_2(OH_2)]^{2+}$ undergoes further oxidation and ligand loss to give RuO_2.[34]

Discussion

Characterization of $[(tpy)(C_2O_4)Ru^{III}ORu^{III}(C_2O_4)(tpy)]\cdot 8H_2O$ (1). The RuORu angle in **1** is 148.5°. This is the smallest angle reported to date for a singly bridged (μ-oxo) complex of Ru^{III} in a series in which ∠RuORu spans the range from 148.5° to 180°.[12,35−37] Further RuORu bending in **1** is inhibited by repulsive tpy−tpy interactions across the RuORu bridge. The separation between the centers of the aromatic ring systems is 3.445 Å.

The Ru−O bonds of the μ-oxo bridge are unusually short. The average is 1.843 Å compared to 1.869 Å in *cis*,*cis*-$[(bpy)_2(H_2O)Ru^{III}ORu^{III}(H_2O)(bpy)_2]^{4+}$ (∠RuORu = 152.2°) and 1.913 Å in $[\{LRu(acac)\}_2(\mu\text{-O})]^{2+}$ (L is 1,4,7-trimethyl-1,4,7-triazacyclononane, ∠RuORu = 180°).[12,35,36] The short Ru−O bonds point to multiple bonding in the RuORu core and strong electronic coupling through a molecular orbital system which spans the two ruthenium centers.

There is a notable asymmetry in the Ru−oxalate binding with the Ru−O bond length *trans* to the bridge shorter (2.080 and 2.067 Å) than *cis* Ru−O (both 2.108 Å). The $Ru-O_{H_2O}$ lengths in the blue dimer are 2.136 Å.[12] In $[\{LRu(acac)\}_2(\mu\text{-O})]^{2+}$,[35] there is an opposite *trans* effect with $Ru-N_{trans}$ 2.148 Å and $Ru-N_{cis}$ 2.097 Å.

The angles between the *trans*-N atoms in the tpy ligand and Ru are considerably less than 180° (159.1° and 159.3°), as expected for Ru(tpy) coordination. This angle is 161.1° in $[Ru^{VI}(tpy)(O)_2(H_2O)]^{2+}$.[8,9] The torsional angle between the plane defined by $O_{21}-Ru_2-O_{22}$ in Figure 1 and the plane defined by $O_{11}-Ru_1-O_{12}$ is 22.7°. Related angles are 65.7° in the blue dimer[12] and 28.45° in $[(bpy)_2(NH_3)Ru^{III}ORu^{III}(NH_3)(bpy)_2]^{4+}$.[38]

Compound **1** is diamagnetic with no paramagnetic influence in the proton NMR spectrum. The $Ru^{III}ORu^{III}$ form of the blue dimer is paramagnetic with a magnetic moment of 1.60 μ_B/dimer at room temperature in the solid state.[37,39] The difference in magnetic behavior is consistent with a qualitative molecular orbital scheme suggested for the blue dimer in which decreasing the RuORu angle increases the splitting between low-lying π^*(RuORu) levels which increased the energy gap between the ground and magnetic excited states.

One-electron oxidation of **1** occurs at 0.73 V (vs NHE) from pH = 4−8 to give $[(tpy)(C_2O_4)Ru^{IV}ORu^{III}(C_2O_4)(tpy)]^{+}$. It is paramagnetic, as expected, as shown by the ^{1}H NMR spectrum, which is relaxed and broadened into the base line in water.

From the ^{1}H NMR spectrum of **1**, the terpyridyl ligands are magnetically equivalent in solution but they are asymmetrical around the torsional axis in the crystal. Either the torsional angle is 0° in solution or, more likely, there is averaging around the torsional axis due to a low barrier to torsional motions.

The UV−vis spectrum of **1** in 1 M $HClO_4$ includes typical $\pi \rightarrow \pi^*$(tpy) bands at 274 and 320 nm and an intense $\pi \rightarrow \pi^*$(RuORu) band at $\lambda_{max} = 640$ nm, $\epsilon = 22\,000$ M^{-1} cm^{-1} compared to 637 nm, $\epsilon = 21\,100$ M^{-1} cm^{-1} for the blue dimer.[12]

$[(tpy)(H_2O)_2Ru^{III}ORu^{III}(H_2O)_2(tpy)]^{4+}$ (2). Compound **1** undergoes hydrolysis on the time scale of minutes in 1 M perchloric or triflic acids to give **2**. The *cis*, *cis* structure at the Ru sites in **1** appears to be maintained with a comparable RuORu angle. ν_{sym}(RuORu) occurs at 474 cm^{-1} compared to 467 cm^{-1} in **1**. In μ-oxo complexes of Fe^{III}, the energies of ν_{sym} and ν_{asym} of the FeOFe core are known to be sensitive to ∠FeOFe with ν_{sym} decreasing with ∠FeOFe.[40] Also, addition of excess sodium oxalate to solutions containing **2** regenerates **1** quantitatively; addition of excess sodium carbonate generates **3**.

There is a single set of tpy resonances in the ^{1}H NMR spectrum of $[(tpy)(H_2O)_2Ru^{III}ORu^{III}(H_2O)_2(tpy)]^{4+}$ showing that, as in **1**, the terpyridyl ligands are in equivalent magnetic environments on the NMR time scale. There is a general shift in the tpy resonances to higher field compared to **1** as expected

(34) The same product appears in solutions containing *cis*,*cis*-$[(bpy)_2(H_2O)Ru^{III}ORu^{III}(OH_2)(bpy)_2]^{4+}$ and Ce^{IV} in large excess as shown by XPS measurements (J. Ni, unpublished observations).

(35) Schneider, R.; Weyhermüller, T.; Wieghardt, K. *Inorg. Chem.* **1993**, *32*, 4925−4934.
(36) Phelps, D. W.; Kahn, E. M.; Hodgson, D. J. *Inorg. Chem.* **1975**, *14*, 2486-2490.
(37) Weaver, T. R.; Meyer, T. J.; Adeyemi, S.; Brown, G. M.; Eckberg, R.; Hatfield, W. E.; Johnson, E. C.; Murray, R. W.; Untereker, D. *J. Am. Chem. Soc.* **1975**, *97*, 3039−3048.
(38) Ishitani, O. Unpublished results.
(39) Dobson, J. C.; Sullivan, B. P, Doppelt, P.; Meyer, T. J. *Inorg. Chem.* **1988**, *27*, 3863−3866.
(40) Sanders-Loehr, J.; Wheeler, W. D.; Shiemke, A. K.; Averill, B. A.; Loehr, T. M. *J. Am. Chem. Soc.* **1989**, *111*, 8084−8093.

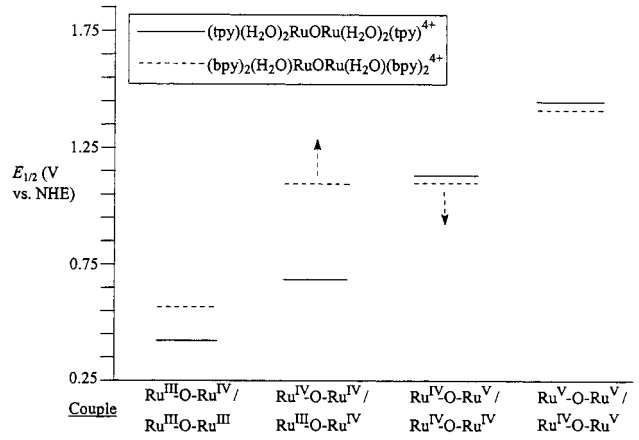

Figure 3. $E_{1/2}$ values at pH 7, $\mu = 0.1$ M versus NHE for $[(tpy)(H_2O)_2RuORu(tpy)(H_2O)_2]^{4+}$ (—) and *cis,cis*-$[(bpy)_2(H_2O)RuORu(bpy)_2(H_2O)]^{4+}$ (- - -). The potentials for couples involving $Ru^{IV}ORu^{IV}$ for the blue dimer are estimates because of its instability with respect to disproportionation. See text.

for substitution of the electron-donating oxalato ligands by aqua ligands. The diamagnetism of **1** is also retained in **2**.

There are three possible structures for **2.** They are labeled in the illustrations below as *cis, cis*; *cis, trans*; and *trans, trans*. The labeling scheme refers to the relative dispositions of the water molecules at each Ru site, *cis* or *trans*. The *cis, cis* structure is most likely for **2** on the basis of the ^{1}H NMR data and the substitution of chemistry with $C_2O_4^{2-}$ which returns **2** to the known *cis, cis* stereochemistry of **1**.

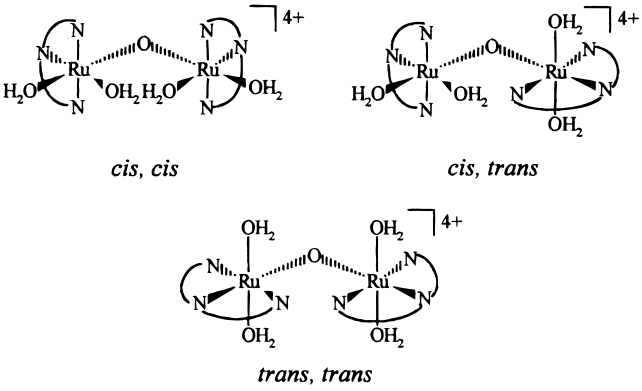

Redox Chemistry. One-electron oxidation of **2** gives paramagnetic $[(tpy)(H_2O)(OH)Ru^{IV}OR(H_2O)_2(tpy)]^{4+}$. In 0.1 M $HClO_4$ the intense $\pi \rightarrow \pi^*$(RuORu) band is shifted from 598 nm in **2** to 472 nm. For the blue dimer, the shift is from 637 to 444 nm.[12] Further one-electron oxidation of $[(tpy)(H_2O)(OH)Ru^{IV}ORu^{III}(H_2O)_2(tpy)]^{4+}$ gives $[(tpy)(H_2O)_2Ru^{IV}ORu^{IV}(H_2O)(OH)(tpy)]^{5+}$ with intense absorption bands at 460 and 380 nm. The redox chemistry of **2** is summarized in the potential−pH diagram in Figure 2.

The redox potential comparison with the blue dimer at pH = 7 in Figure 3 reveals the following: (1) two-electron reduction from $Ru^{III}ORu^{III}$ to $Ru^{II}ORu^{II}$ occurs for both at 0.10 V versus NHE at pH 7. (2) Oxidation of $Ru^{III}ORu^{III}$ to $Ru^{IV}ORu^{III}$ occurs at 0.41 V for **2** and at 0.55 V for the blue dimer. (3) Oxidation of $Ru^{IV}ORu^{III}$ to $Ru^{IV}ORu^{IV}$ occurs at 0.66 V and of $Ru^{IV}ORu^{IV}$ to $Ru^{V}ORu^{IV}$ at 1.13 V for **2**. $E_{1/2} = 0.90$ V for the two-electron $Ru^{IV}ORu^{IV}/Ru^{III}ORu^{III}$ couple. For the blue dimer, oxidation of $Ru^{IV}ORu^{III}$ occurs by a single two-electron wave to give $Ru^{V}ORu^{IV}$ at 1.09 V. (4) For **2**, $Ru^{IV}ORu^{IV}$ is stable with respect to disproportionation into $Ru^{IV}ORu^{III}$ and $Ru^{V}ORu^{IV}$ by 0.24 V.

Chart 1

reaction	pH	$\Delta G°'$, eV
$Ru^{V}ORu^{V}$		
2 V-V + 2 H_2O → 2 IV-IV + O_2 + 2 H^+	1	-1.24
V-V + 2 H_2O → III-III + O_2 + 2 H^+	1	-0.08
V-V + 2 H_2O → IV-IV + H_2O_2 + H^+	1	0.46
2 V-V + 2 H_2O → 2 V-IV + H_2O_2 + 4 H^+	7	-0.16
V-V + 2 H_2O → IV-IV + H_2O_2 + 2 H^+	7	0.14
2 V-V + 2 H_2O → 2 IV-IV + O_2 + 2 H^+	7	-1.88
V-V + 2 H_2O → III-III + O_2 + H^+	7	-0.36
$Ru^{IV}ORu^{V}$		
2 V-IV + 2 H_2O → 2 IV-III + O_2	7	-0.32
V-IV + 2 H_2O → IV-III + H_2O_2	7	0.92
$Ru^{IV}ORu^{IV}$		
2 IV-IV + 2 H_2O → 2 III-III + O_2 + 2 H^+	1	1.08
IV-IV + 2 H_2O → III-III + H_2O_2 + H^+	1	1.62
2 IV-IV + 2 H_2O → 2 III-III + O_2	7	1.12

The $Ru^{IV}ORu^{IV}$ form of the blue dimer is unstable with respect to disproportionation. (This means that $E_{1/2}$ for the $Ru^{IV}ORu^{IV}/Ru^{IV}ORu^{III}$ couple is *higher* than $E_{1/2}$ for the $Ru^{V}ORu^{IV}/Ru^{IV}ORu^{IV}$ couple, and $E_{1/2}(Ru^{IV}ORu^{IV}/Ru^{IV}ORu^{III}) > 1.09$ V and $E_{1/2}(Ru^{V}ORu^{IV}/Ru^{IV}ORu^{IV}) \leq 1.09$ V.) (5) One-electron oxidation of $Ru^{V}ORu^{IV}$ to $Ru^{V}ORu^{V}$ occurs at 1.44 V for **2** and at 1.40 V for the blue dimer. (6) At pH ≥ 2, $Ru^{V}ORu^{IV}$ is unstable with respect to disproportionation into $Ru^{V}ORu^{V}$ and $Ru^{IV}ORu^{IV}$. ($E_{1/2}(Ru^{V}ORu^{IV}/Ru^{IV}ORu^{IV}) > E_{1/2}(Ru^{V}ORu^{V}/Ru^{V}ORu^{IV})$.) Past this pH, $Ru^{V}ORu^{IV}$ is the strongest oxidant in the system, thermodynamically more potent than $Ru^{V}ORu^{V}$. For the blue dimer, a similar crossover of the $Ru^{V}ORu^{V}/Ru^{V}ORu^{IV}$ and $Ru^{V}ORu^{IV}/Ru^{IV}ORu^{III}$ couples occurs at pH ≈ 2.

The difference in potentials between **2** and the blue dimer at pH = 7 is illustrated graphically in Figure 3 (see also Supporting Information). This representation of the data reveals clearly the two significant differences between them. One is the increase in $E_{1/2}$ for the $Ru^{IV}ORu^{III}/Ru^{III}ORu^{III}$ and $Ru^{IV}ORu^{IV}/Ru^{IV}ORu^{III}$ couples for the blue dimer. The other is the instability of $Ru^{IV}ORu^{IV}$ toward disproportionation. An important contribution to these differences may be structural, arising from a difference between ∠RuORu bond angles. The role of bridge angle on redox properties is currently under investigation in a series of μ-oxo dimers.

Water Oxidation. Water oxidation by the oxidized forms of **2** is thermodynamically feasible, but only for certain of the higher oxidation state couples. Relevant potentials are presented in Supporting Information Table S1 as formal potentials ($E_{1/2} \approx E^{\circ\prime}$). On the basis of these potentials and those for relevant O_2/H_2O couples, values of $\Delta G^{\circ\prime}$ for reactions that may be of relevance to water oxidation are listed in Chart 1 at pH = 1

Scheme 2

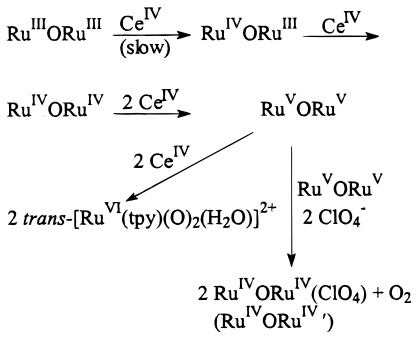

and 7. For convenience, the oxidation states are labeled as V−V for $Ru^{V}ORu^{V}$ etc.

A number of conclusions can be reached from these calculations: (1) Direct, four-electron oxidation of water to O_2 by the $Ru^{V}ORu^{V}/Ru^{III}ORu^{III}$ couple is spontaneous at either pH. Two-electron oxidation to H_2O_2 is nonspontaneous. (2) For $Ru^{V}ORu^{V}$, bimolecular pathways are thermodynamically more favored for oxidation of H_2O, either to O_2 or to H_2O_2. At pH = 7, even the $Ru^{V}ORu^{IV}$ form of the dimer is thermodynamically capable of oxidizing water to dioxygen. (3) The $Ru^{IV}ORu^{IV}$ form of the dimer is thermodynamically incapable of oxidizing water at either pH.

Although water oxidation by Ce^{IV} occurs in solutions to which **2** has been added, the reaction is not truly catalytic, as shown by the data in Table 5. A number of observations give insight into the mechanism of water oxidation and why **2** is limited in its ability to oxidize water catalytically: (1) Oxidation of $Ru^{IV}ORu^{IV}$ by Ce^{IV} does give O_2, but the metal complex products are $[Ru^{VI}(tpy)(O)_2(OH_2)]^{2+}$ and $Ru^{IV}ORu^{IV}{}'$. $Ru^{IV}ORu^{IV}{}'$ does not undergo further oxidation with added Ce^{IV}. (2) Under a variety of conditions with Ce^{IV} added to solutions of **2**, O_2 evolution per dimer does not exceed 1 (Table 5). (3) $Ru^{IV}ORu^{IV}{}'$ and O_2 are favored as products over $Ru^{VI}(tpy)(O)_2(OH_2)^{2+}$ as the initial $Ru^{IV}ORu^{IV}$ concentration is increased.

A series of reactions that can explain these results is shown in Scheme 2. Scheme 2 invokes two complications that prevent catalytic water oxidation. One is "overoxidation" of $Ru^{V}ORu^{V}$ to $[Ru^{VI}(tpy)(O)_2(OH_2)]^{2+}$ which is in competition with O_2 evolution. ($Ru^{V}ORu^{V}$ is presumably $[(tpy)(OH_2)(O)Ru^{V}ORu^{V}(O)(OH_2)(tpy)]^{4+}$.) There is precedence for this reaction in the overoxidation of *cis,cis*-$[(bpy)_2(O)Os^{V}OOs^{V}(O)(bpy)_2]^{4+}$ to give $[Os^{VI}(O)_2(OH)_2(bpy)]$.[14] In both cases, the driving force is the electronic stabilization associated with formation of the d^2 *trans*-dioxo M^{VI} core.

The second limiting factor is that the coproduct of O_2 evolution is $Ru^{IV}ORu^{IV}{}'$ rather than $Ru^{IV}ORu^{IV}$. This is limiting because $Ru^{IV}ORu^{IV}{}'$ is not further oxidized by Ce^{IV} and is removed from the catalyst pool. Products related to $Ru^{IV}ORu^{IV}{}'$ are observed following oxidation of the blue dimer or *cis,cis*-$[(L)_2(H_2O)Ru^{III}ORu^{III}(OH_2)(L)_2]^{4+}$ (where L = 2,2′-bipyridine, 4,4′-dicarboxy-2,2′-bipyridine, or 5,5′-dicarboxy-2,2′-bipyridine). They have been attributed to anated forms which appear upon water oxidation.[41] In $Ru^{IV}ORu^{IV}{}'$, the basic μ-oxo structure is retained, and it is presumably also an anated form. Assuming this to be the case, reduction to $Ru^{III}ORu^{III}$ results in labilization of the anion and reappearance of **2**,

$$Ru^{IV}ORu^{IV}(ClO_4) \xrightarrow{+2e^-} Ru^{III}ORu^{III}(ClO_4) \xrightarrow[-ClO_4^-]{+H_2O} Ru^{III}ORu^{III} \quad (12)$$

We have no spectroscopic information about how ClO_4^- or $CF_3SO_3^-$ is bound. It was not possible to apply in situ resonance Raman spectroscopy because of the photosensitivity of $Ru^{IV}ORu^{IV}$ in solution.

Spontaneous anation of $Ru^{IV}ORu^{IV}$ does not occur even over a period of hours. Anation is triggered by oxidation and O_2 evolution, perhaps by capture of a lower coordinate intermediate by an ion-paired counterion.

There is additional information in the mixing experiments with Ce^{IV}. Water oxidation and $Ru^{IV}ORu^{IV}{}'$ are favored over *trans*-$[Ru^{VI}(tpy)(O)_2(H_2O)]^{2+}$ as the initial $Ru^{IV}ORu^{IV}$ concentration is increased. This points to a possible bimolecular mechanism for water oxidation which is incorporated into Scheme 2.

Addition of 1−10 equiv of Ce^{IV} to $Ru^{III}ORu^{III}$ results in some O_2 evolution and mixtures of $Ru^{III}ORu^{III}$ and $Ru^{IV}ORu^{III}$. $Ru^{IV}ORu^{IV}$ is *not* observed. This points to Ce^{IV} oxidation of $Ru^{III}ORu^{III}$ to $Ru^{III}ORu^{IV}$ as a slow step with further oxidation rapid. Because of this, O_2 is produced with as little as 1 equiv of Ce^{IV}.

Comparisons with the Blue Dimer. At the end of this paper it seems appropriate to compare the properties of **2** and the blue dimer. In both, the RuORu bridge is maintained, but in **2** there are two water molecules at each Ru rather than one. The effect of this change on the thermodynamics is significant. At pH 7 the blue dimer is stabilized toward oxidation of $Ru^{III}ORu^{III}$ to $Ru^{IV}ORu^{III}$ by 0.14 V. It is stabilized toward further oxidation to $Ru^{IV}ORu^{IV}$ by >0.43 V. This remarkable stabilization of $Ru^{IV}ORu^{III}$ toward further oxidation (or destabilization of $Ru^{IV}ORu^{IV}$) results in a lower potential for oxidation to $Ru^{V}ORu^{IV}$ and causes the instability of $Ru^{IV}ORu^{IV}$ toward disproportionation. In **2**, there is a progressive increase in $E_{1/2}$ for the one-electron $Ru^{IV}ORu^{III}/Ru^{III}ORu^{III}$ and $Ru^{IV}ORu^{IV}/Ru^{IV}ORu^{III}$ couples. $Ru^{IV}ORu^{IV}$ is a stable oxidation state, stable toward disproportionation and incapable of oxidizing water to O_2.

The presence of two water molecules per Ru in **2** has a deleterious effect on catalyst stability. This arises from overoxidation past $Ru^{V}ORu^{V}$ to give *trans*-$[Ru^{VI}(tpy)(O)_2(H_2O)]^{2+}$. Stabilization of Ru^{VI} by *trans*-dioxo formation is required, and its accessibility is tied to the presence of the two water molecules in each coordination sphere.

Acknowledgment is made to the National Science Foundation under Grant CHE-9503738 and the National Institutes of Health under Grant 5-R01-GM32296-11 for support of this research. We also acknowledge Dr. Chris Chronister and Dr. Luis Baraldo for their helpful discussions and assistance with experimental measurements.

Supporting Information Available: Tables listing calculated redox potentials of **2** and detailed crystallographic data, atomic positional parameters, and bond lengths and angles of **1** (13 pages). Ordering information is given on any current masthead page.

IC970908Z

(41) Rotzinger, F. P.; Munavalli, S.; Comte, P.; Hurst, J. K.; Grätzel, M.; Pern, F. J.; Frank, A. J. *J. Am. Chem. Soc.* **1987**, *109*, 6619−6626.